PROGRESS IN SILICON SOLAR CELL CHARACTERIZATION WITH INFRARED IMAGING METHODS

M. Kasemann[1], W. Kwapil[1], B. Walter[1], J. Giesecke[1], B. Michl[2], M. The[1], J.-M. Wagner[3], J. Bauer[3], A. Schütt[4], J. Carstensen[4], H. Kampwerth[5], P. Gundel[1], M.C. Schubert[1], R.A. Bardos[6], H. Föll[4] H. Nagel[2], P. Würfel[7], T. Trupke[5], O. Breitenstein[3], W. Warta[1], S.W. Glunz[1]
[1] Fraunhofer Institute for Solar Energy Systems (ISE), Heidenhofstr. 2, 79110 Freiburg, Germany
Phone: +49 761 4588-5321, e-mail: martin.kasemann@ise.fraunhofer.de
[2] SCHOTT Solar GmbH, Carl-Zeiss-Straße 4, 63755 Alzenau, Germany
[3] Max Planck Institute for Microstructure Physics, Weinberg 2, 06120 Halle, Germany
[4] University of Kiel, Kaiserstr. 2, 24143 Kiel, Germany
5 The University of New South Wales, Sydney, 2052, NSW, Australia
[6] BT Imaging Pty Ltd, 18 Bulletin Place, Sydney, 2000, NSW, Australia
[7] Insititut für Angewandte Physik, Universität Karlsruhe, Germany

ABSTRACT: This paper reviews the latest results in application and development of infrared imaging methods for fast and spatially resolved silicon solar cell characterization. Infrared imaging methods comprise electroluminescence (EL) imaging, photoluminescence (PL) imaging, and lock-in thermography (LIT). We report on new insights into the nature of local series resistances and important observations on local junction breakdown in industrial multi-crystalline silicon solar cells. Significant improvements have been achieved in the applicability of infrared imaging methods for in-line application in silicon solar cell production. It was demonstrated that quantitative values for local reverse currents in hot-spots can be easily obtained in 10 milliseconds. Quantitative series resistance images were obtained in 800 milliseconds with a good potential to reduce the measurement time to below 500 milliseconds.
Keywords: Characterisation, Electrical Properties, Imaging

1 INTRODUCTION

With the development of fast and low-noise charge coupled device (CCD) detectors in different wavelength ranges, infrared imaging methods have found numerous potential applications in spatially resolved solar cell characterization and production quality control.[1]

In this paper we review the highlights of the progress in infrared imaging method development that was made during the last year. Significant improvements have been achieved in the applicability of infrared imaging methods for in-line process control in silicon solar cell production. It was demonstrated that quantitative values for local reverse currents in hot-spots can be easily obtained in 10 milliseconds. Quantitative series resistance images were obtained in 800 milliseconds with a good potential to reduce the measurement time to below 500 milliseconds.

We also report on new insights into the nature of local series resistances and important observations on local junction breakdown in industrial multi-crystalline silicon solar cells.

2 METHOD OVERVIEW

The basic setup used for infrared imaging methods is shown in Figure 1a. The solar cell is mounted on a (temperature controlled) measurement chuck and electrically contacted to a power supply/load. In measurement modes where illumination is required, the cell is typically irradiated with lasers in the wavelength range of 790 nm to 940 nm. For measurements on wafers and for lock-in thermography measurements on cells, the sample is sometimes irradiated from the back side. Different commercially available charge coupled device (CCD) cameras can be used to image the radiation emitted by the solar cell. Optical filters can be additionally applied in order to observe different parts of the spectrum.

The spectrum emitted by a silicon solar cell, and the underlying mechanisms, are schematically shown in Figure 1b. Band-to-band luminescence is emitted during a radiative recombination event of an electron and hole

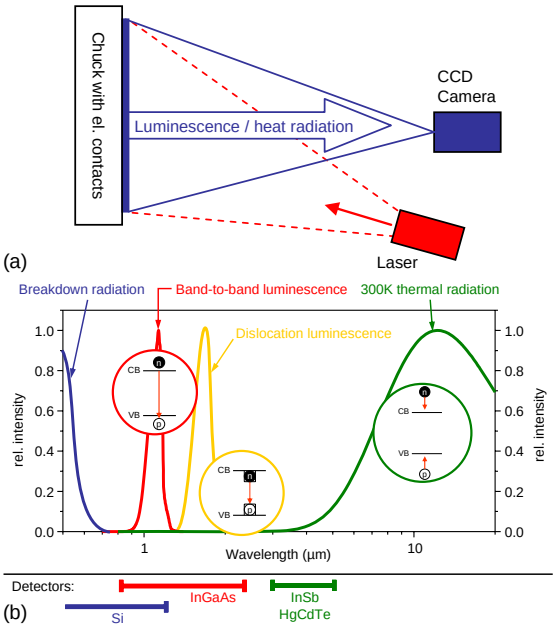

Figure 1: (a) Infrared imaging setup. Homogeneous irradiation of the entire solar cell is typically performed with lasers in the wavelength range from 790 nm to 940 nm. Different cameras can be used to detect radiation in different wavelength ranges. (b) Spectral range of photon emission from silicon solar cells, the underlying mechanisms, and the detectors used in this contribution.

Parameter	Spectrum	Method	Short description	Ref.
Lifetime / Diffusion length	Thermal	CDI or ILM	Carrier Density Imaging/Infrared Lifetime Mapping on wafers. Signal ~ excess carrier density	[5, 6]
	B2B lum.	PLI	PL imaging of wafers. Signal ~ product of electron and hole concentrations, i.e. ~ excess carrier density at low injection.	[7]
	B2B lum.	ELI	EL images through different filters using effects of photon reabsorption to determine carrier profile.	[8]
	B2B lum.	PLI	PL images through different filters using effects of photon reabsorption to determine carrier profile.	this paper
	Thermal	Voc-ILIT	ILIT Signal on cells and diffused wafers under open circuit conditions ~ to dark saturation current.	[9]
Interstitial iron	B2B lum.	PLI	Measure lifetime before and after dissociation of FeB at injection levels below or above the crossover point.	[10]
Dislocations	Defect lum.	ELI or PLI	EL or PL signal between approx. 1.2µm and 1.6µm from recombination via dislocation states in the band gap	[11]
Trapping	Thermal	CDI or ILM	CDI/ILM signal dominated by trapping at low injection. Quantitative determination of trap density.	[12, 13]
Emitter sheet resistance	Thermal	SRI	Sheet resistance imaging. Thermal emission signal ~ free carrier density	[14]
Junction capacitance	Thermal	ICM	Infrared Capacitance Mapping. Thermal emission signal ~ free carrier density. SCR width modulation by reverse bias modulation	[15]
Series resistance	B2B lum.	Rs-PLI	Different PL images. Determines Rs near MPP	[16]
	B2B lum.	Rs-ELI	Rs from derivative of local EL signal with respect to terminal voltage	[17]
	B2B lum.	RESI	Local voltage from EL, local current from DLIT and EL → Rs	[18]
	Thermal	Jsc-ILIT	Qualitative image affected by: 1) High signal due to heating in lateral Rs. 2) Low signal due to decreased thermalization over the junction.	[19]
	Thermal	Rs-DLIT	Division of two DLIT images taken at two different forward biases well above 0.5V	[20]
	Thermal	Rs-ILIT	Combination of MPP and Jsc image. Rs appearance affected by same processes as Jsc-ILIT.	[20]
Shunts	Thermal	ILIT or DLIT	Signal near ~0.5V or MPP dominated by heat dissipation in shunt. Different quantification methods.	[21]
	B2B lum.	PLI or ELI	Low intensity around shunt due to reduction of local junction voltage, caused by voltage drops over series resistances surrounding the shunt.	[22]
Junction breakdown	Thermal	TC-DLIT	Local temperature coefficient of breakdown current	[23]
	Thermal	MF-ILIT	Local current multiplication factor	[23]
	Thermal	Slope-DLIT	"Hardness" of breakdown	[23]
	Visible + NIR		Small light spots in breakdown regions attributed to microplasma radiation and possible other effects.	[1]
Hot spots	Thermal	DLIT	DLIT at reverse voltage (e.g. -10V). Measures local heat dissipation or local current in relevant hot spots in 10 milliseconds.	[1]
Local efficiency	Thermal	MPP-ILIT	Signal ~ total power loss.	[9]
	Thermal	ILIT	Jsc-ILIT image minus MPP-ILIT image divided by Jsc-ILIT image gives local solar cell efficiency if not dominated by Rs.	[24]

Table 1: List of imaging methods for the measurement of different silicon solar cell parameters. Typical abbreviations are: ELI=electroluminescence imaging; PLI=photoluminescence imaging; DLIT=dark lock-in thermography; ILIT=illuminated lock-in thermography; MPP=maximum power point; Jsc=short-circuit operating point; Voc=open circuit operating point; Rs=series resistance; NIR = near infrared; B2B=band-to-band; RESI=recombination current and series resistance imaging; SCR = Space Charge Region; TC = Temperature Coefficient

over the band gap. The spectrum is located around 1.1 µm in silicon. Band-to-band luminescence can be detected with silicon sensors and with InGaAs sensors. Light emission has also been observed in a band from approximately 1.2µm to 1.6µm. It is generated by radiative recombination via dislocation states in the band gap. [2, 3] This dislocation luminescence can be detected with an InGaAs sensor combined with properly designed optical band pass filters. The methods based on lock-in thermography (LIT) detect heat radiation emitted by the solar cell close to room temperature. Typical sensor materials for the detection of heat radiation are InSb and HgCdTe. During junction breakdown, light in the visible wavelengths range below approximately 880 nm down through the visible range is often observed. [4]

Many different IR imaging methods for the spatially resolved detection of different electrical properties have already been proposed. These methods are based on different detection principles, they work in different production states and in different operating modes of the solar cell. A comprehensive list of accessible parameters and existing methods is given in Table 1.

3 DIFFUSION LENGTH IMAGING

Typical well-established measurement methods for minority carrier lifetimes and diffusion lengths were Light-Beam Induced Current (LBIC), local PhotoConductance Decay measured by the Microwave Reflectivity (MW-PCD), and Modulated Free Carrier Absorption. These methods have several disadvantages, the most severe being the low speed due to scanning procedures. One of the first infrared imaging methods for lifetime measurements were infrared lifetime imaging (ILM) and carrier density imaging (CDI). [5, 6] Both methods are based on extracting the excess carrier density from measurements of the generation-dependent free carrier absorption or emission. A major disadvantage of these methods are the high sample temperatures required for sufficient heat radiation emission, and especially the existence of "trapping" artifacts under low injection conditions. Over the last years, methods based on photoluminescence imaging have been developed that are able to measure lifetime distributions in silicon wafers in very short measurement times. The quantification of the resulting images is more difficult than e.g. for CDI images. Currently the most widely used method is to calibrate a section of a luminescence image against a quasi-steady-state photoconductance measurement for each measured wafer.

Only recently, a new electroluminescence-based method for minority carrier diffusion length measurements has been proposed that does not require a calibration. This method has been shown to yield very good quantitative agreement with LBIC.[8] The essential working principle of this method is based on the reabsorption of generated luminescence photons on their way out of the sample. [25] As illustrated in Figure 2, the spectrum detected from charge carrier recombination events at the rear of the base of the solar cell is significantly shifted (and reduced) compared to the spectrum detected from band-to-band recombination events near the front of the base. Both, the spectrum of luminescence emission by radiative band-to-band recombination in silicon [26], and the processes leading to reabsorption of the generated luminescence photons, are very well understood. An accurate extraction of the depth-dependent carrier profile from the detected luminescence spectrum is thus in principle possible and with it the determination of the minority carrier diffusion length. In a specific realization, Würfel et al.[8] used two short-pass filters at different wave-lengths to obtain two images with different spectral information. They divided the two images and compared each pixel to a calculated calibration curve for this quotient from a simulation of the expected excess carrier profile in dependence of the diffusion length. Every pixel of the quotient image was calibrated according to this calibration curve to yield a local diffusion length which correlated very well with LBIC. The disadvantage of using EL images for this procedure is that only finished cells can be measured, since the excess carriers in the base are electrically injected via the p-n junction.

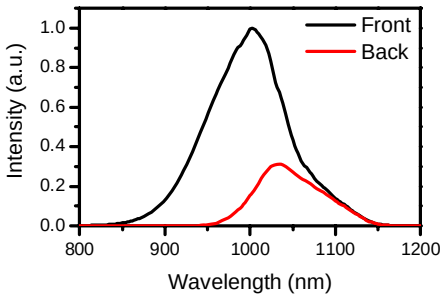

Figure 2: Influence of reabsorption of luminescence photons on the spectrum detected by the camera CCD (i.e. the luminescence emission spectrum is already convoluted with the spectral sensitivity of the CCD). The spectrum emitted from point at the front of a 300 µm thick silicon wafer differs significantly from the spectrum emitted by a point at the back of the wafer.

In order to measure diffusion lengths earlier in the solar cell production process, it is desirable to transfer this evaluation method to photoluminescence images. In a more detailed contribution to this conference, we describe how this transfer is made.[27] The experimental complexities that arise with this method are described in more detail there. Our experiments have shown the following: (1) an exact knowledge of the spectral characteristics of the different optical devices in the optical path between the solar cell and the CCD detector is crucial for obtaining correct diffusion length values. The values available from calibration measurements of optical device providers were mostly not of sufficient accuracy but had to be re-calibrated by ourselves. (2) If the sample is measured from the irradiated side, as shown in Figure 1a, generation light that is reflected by the wafer surface leads to severe problems. The intensity of the reflected generation light can be orders of magnitude higher than the luminescence intensity that needs to be measured. Long pass filters that suppress the reflected generation light by orders of magnitude (and leave the luminescence light unaltered) are available but often generate fluorescence by themselves. We solved this problem in two ways: First, by developing a reflection correction method, and second, by irradiating the wafer from the back side and detecting the emitted luminescence from the front side.

4 LOCAL JUNCTION BREAKDOWN

Module operating conditions can likely occur, where a solar cell is operated at reverse voltages around 10V. Figure 3a shows that even at such low reverse voltages the junction can already break down locally, although the theoretical junction breakdown voltage of an industrial silicon solar cell with typical base doping densities around 10^{16} cm^{-3} should be around -50V. Under these conditions, the local heating at breakdown sites can easily lead to hot spots with peak temperatures of several hundred degree centigrade that can damage the cell and the module. [28] In further investigations we have found that several different local breakdown mechanisms are acting in mc silicon solar cells at low reverse voltages between 7 and 15 V. In this paper, we give a short overview over the different observations and probable breakdown processes. A more detailed discussion of our findings can be found in other contributions to this conference. [29, 30]

The detailed investigation on local junction breakdown were performed mainly by applying several new DLIT techniques that have recently been proposed by

some of the authors. [23] The techniques comprise a method for the determination of the local temperature coefficient of the breakdown current (TC-DLIT), a method to determine the local current multiplication factor in avalanche breakdown (MF-ILIT), and a method to determine the "hardness" of the breakdown (Slope-DLIT).

There are three basic mechanisms for junction breakdown, namely thermal breakdown, Zener breakdown, and avalanche breakdown. [31] Thermal breakdown occurs if the junction temperature becomes so high that silicon becomes intrinsically conductive. For Zener breakdown, the band configuration at the junction must allow for tunneling processes from the conduction band in the n-doped region into the valence band in the p-doped region. This process requires (locally) narrow p-n-junctions, while in wider p-n-junctions, the effect of avalanche breakdown is more likely. In the latter case, a generated electron is accelerated from the p-side to the n-side of the junction by the electric field. If the electric field increases above a certain threshold value, the kinetic energy of the accelerated electron is sufficient to generate an electron-hole-pair by impact ionization within the junction. These additional free carriers now contribute to the current and can in turn generate other carrier pairs by impact ionization. This avalanche process causes the junction to become conductive in reverse bias. The breakdown current in avalanche breakdown typically decreases with increasing temperature because the maximum kinetic energy achievable by an electron in the junction is limited by collisions with the crystal lattice. These collisions are more likely towards higher crystal temperatures due to the increased thermal movement of lattice atoms. The opposite temperature-dependence is expected for Zener breakdown since the band gap gets narrower with increasing temperature.

As shown in Figure 3a, some regions start to break down at around 8V reverse bias. These breakdown sites show a significantly negative temperature coefficient (not shown) but an almost linear reverse current-voltage curve as shown in Figure 3d. The mechanism behind these early breakdown sites is not clearly identified yet.

A second class of breakdown sites is observed around 13V reverse bias (Figure 3b). These breakdown regions exhibit a soft breakdown characteristic (Figure 3d) and only a slightly negative temperature coefficient (not shown). Measurements on material defects and dislocation luminescence indicate the existence of decorated dislocations in these regions, while no local breakdown was observed at clean dislocations. [1, 32] The impurities decorating the dislocations are assumed to generate trap centres deep in the band gap. These traps can promote trap-assisted breakdown processes in the junction under reverse bias. Trap-assisted tunnelling (with probable subsequent avalanche) is currently seen as the most likely process for breakdown in the respective regions.

A third class of breakdown regions appears at reverse voltages close to 14V (Figure 3c). These regions exhibit a hard breakdown characteristic (Figure 3d) and a clearly negative temperature coefficient (not shown). Both features clearly indicate avalanche breakdown in these regions. Further investigations showed that etching holes in the wafer surfaces, brought in during the acidic texturing process, are responsible for these breakdowns.

Our investigations on junction breakdown have two main implications: (1) The clear correlation of avalanche

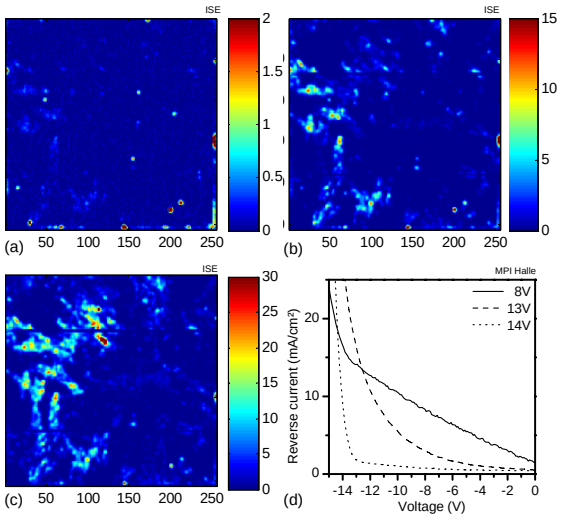

Figure 3: Measurements on local junction breakdown in multi-crystalline silicon solar cells. Images of the local power dissipation (a) at 8V reverse bias showing spots of very early breakdown, (b) at 13V reverse bias, showing entire areas of early breakdown, and (c) at 14V reverse bias, showing a number of additional breakdown regions compared to (b). (d) More detailed measurements of the reverse current-voltage curve in different selected regions. The "8V"-curve relates to regions breaking down at 8V reverse bias and so on. (ISE and MPI)

breakdown sites and etching hole distributions shows that the formation of surface faults during acidic texturing must be understood and eliminated. (2) Preferential breakdown at decorated dislocations may lead to new challenges in connection with the trend towards enabling the production of silicon solar cells from high-impurity feedstock. [33] There, specially designed temperature processes that cause a diffusion of free impurity species from the bulk material towards dislocation networks (where they precipitate) are currently seen as an efficient means to reduce the overall recombination activity in the solar cell under forward bias. [33] According to our discussion, however, the decorated dislocations might then break down at low reverse voltages which could cause significant hot-spot problems in solar cell operation. To avoid such problems (and others), methods for the effective electrical isolation of decorated dislocations (and shunts) should be given more attention. [34]

5 HOT SPOT DETECTION IN 0.01 SECONDS

As mentioned before, module operating conditions can likely occur, where solar cells are operated at reverse voltages around 10V. Under these conditions, local heating in "hot spots" caused by local breakdown or shunts can damage the cell and the module.[28] Today, the appearance of hot spot in solar cells is mostly deduced from the global shunt resistance or the global reverse current at 10V reverse bias. But this global information is only of limited use since the local current *density* or local power *density* is much more important for localized hot spot appearance than the corresponding global values. Spatially resolved information is thus especially valuable in this case. A spatially resolved method for hot-spot detec-

tion that has recently surfaced in industrial production control is based on measuring the (equilibrium) temperature distribution on the cell by means of thermography. This approach has three disadvantages: (1) The temperature distribution is completely different on an isolated cell than in the laminated module. (2) The spatial resolution of such a measurement is very poor. (3) The time needed to reach a (reproducible and stable) equilibrium temperature distribution is long compared to the typical station times.

Only very recently, however, some of the authors proposed a very simple and ultra-fast DLIT method for quantitative hot-spot detection in an industrial production line.[1] Typical measurement times are in the order of only 10 milliseconds, which could be fast enough to get spatially resolved information about the local reverse current during a standard reverse current measurement in a typical industrial I-V-curve tester. The method is based on dark lock-in thermography which gives an image of the lateral distribution of the locally dissipated power density. [35] The local power density can be transformed into the local current density under the assumption of a laterally constant reverse voltage across the cell. [36] Both values, the locally dissipated power density and the local reverse current density, are a reliable and meaningful quantitative measure for hot spot appearance since they determine the final temperature distribution in the module. The resulting image can be automatically evaluated with preset threshold values and a subsequent automated decision for further processing can be made. Recent experiments (performed with the cell under forward bias) indicate, for example, that shunts can be effectively isolated from the rest of the cell by laser scribing. [34]

Figure 4 shows an image of the reverse current distribution at 10V reverse bias in an intentionally shunted solar cell. The image was obtained in 10 milliseconds according to the procedure described in Ref. [1]. The measurement shows that localized spots (with a diameter of approximately 50 to 100 µm) that carry more than 120 mA reverse current can be easily resolved. Measurements of the same cell at lower reverse biases show that hot spots can be detected in 10 milliseconds as soon as the local reverse current in localized hot spots exceeds approximately 10 mA.

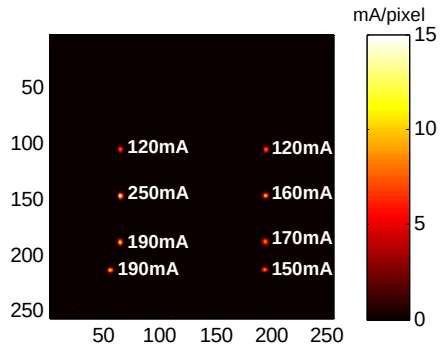

Figure 4: Image of the local reverse current at 10 V reverse bias. The image was taken in 10 milliseconds on an intentionally shunted solar cell. (ISE)

6 SERIES RESISTANCE IMAGING IN 0.8 S

The series resistance is one of the most important parameters determining the efficiency of industrial solar cells. An increase of 1 Ωcm² in the global series resistance typically leads to an absolute fill factor loss of approximately 5%. [37] Already the determination of the global series resistance is non-trivial, but almost three decades of research have produced several useful methods to measure the global series resistance.[37] However, the global series resistance value alone gives only limited information about possible *causes* for increased series resistances. The knowledge of where on the cell potential problems of increased series resistance are located, helps a lot in identifying possible causes and taking appropriate countermeasures. Up to now, an offline method called Corescan is often used for these purposes. Unfortunately, this method destroys the cell and is comparably slow, with typical measurement times of several minutes.

Only recently, several fast and non-destructive methods for the determination of local series resistances have been proposed.[16-18] The methods are based on luminescence imaging techniques. Trupke et al. [16] have proposed a method which measures the local series resistance based on several PL images under different conditions. We refer to this method as "Rs-PLI". Ramspeck et al. [18] have proposed a method called "RESI" (REcombination current and Series resistance Imaging) which obtains the lateral voltage distribution on the cell from an EL image, while obtaining the local current from a combination of a DLIT image and an EL image. Hinken et al. [38] have proposed a method based on several EL images using a derivative-method originally proposed by Werner et al. for current-voltage curve evaluation of diodes [39]. We reference this method as "Rs-ELI".

The basic thinking model behind all of the above methods is that every pixel of the solar cell is connected to the cell terminal via a single series resistance. This results in a schematic solar cell model shown in Figure 5a. Figure 5b reveals more details behind this definition of the local series resistance, showing a schematic model for the flow of majority carriers between two fingers. From this schematic, it is obvious that the local series resistance "R_S", which is defined for each pixel, is actually a lumped series resistance consisting of partial contributions from each of the foregoing elements in the current path. As the foregoing elements are not made up of entirely linear elements (like ohmic resistances) it is obvious that the resulting local series resistance will be injection-dependent. Our simulations of more detailed solar cell models have shown that the non-linearity of the local series resistance is critical for voltages above the maximum power point, both for EL-based methods as well as PL-based methods. [40] For measurements below the maximum power point, the model in Figure 5a is a good representation of the majority carrier flow in solar cells.

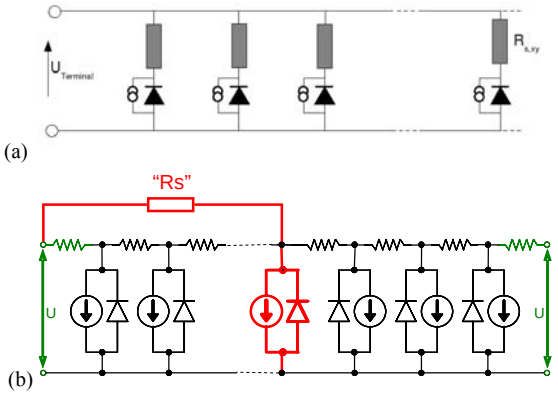

Figure 5: Schematic model of local series resistances (a) according to the definition used for present luminescence imaging techniques, (b) according to a model representing the current flows more realistic.

The relation between the local series resistance (defined according to Figure 5a) and the global series resistance is investigated in detail in Ref. [40]. From simple current path arguments it is already clear that a series resistance value determined under dark conditions is never representative for the series resistance occurring under operating conditions of the solar cell. [37, 41] This holds for global series resistance determination as well as for local series resistance determination. [1] Therefore, we concentrate on finding a relation between the local series resistances determined by photoluminescence imaging (R_S-PLI) and the global series resistance determined by reliable methods for global series resistance determination. As a critical touchstone we define the correlation of both values with the global fill factor which determines the solar cell efficiency in the end. Different approaches of averaging the local series resistance values have been proposed by different authors, namely an averaging of the conductivities [16] and an averaging of the resistivities [18], both without further motivation or discussion. It was shown by Carstensen et al. [42] that the averaging of local series resistances is correct as long as the local diode resistivities are much higher than the local series resistivities. Accordingly, our experiments and simulations have shown that the averaging of local series resistances gives significantly better results than the averaging of local series conductivities. But despite this, even the (arithmetic) averaging of local series resistances yields significant deviations from the global series resistance in many experiments. Ways to bypass the weaknesses of both averaging methods are discussed in more detail in Ref. [40].

Measurement *speed* is a major issue in industrial application. Therefore, we put efforts into testing cameras with different silicon CCD technologies. The images shown in Figure 6 were taken with a camera employing a certain technique to significantly enhance the quantum efficiency in the spectral range around 1000nm, which is the important range for silicon luminescence detection. As you can see in Figure 6b, we obtained reliable R_S-PL images with a good signal to noise ratio in **0.8 seconds**, which is more than sufficient for inline application. The measurement time could even be significantly reduced by reducing the readout time of the CCD sensor. In our measurements, we had to use a total frame integration time of 400ms for the four images that are necessary to

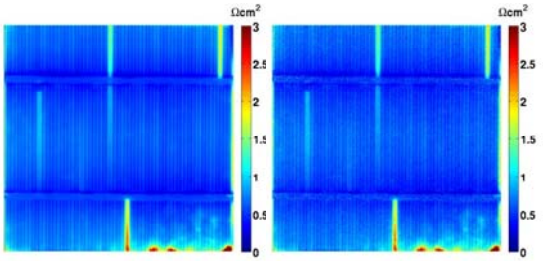

*Figure 6: Fast R_S-PL measurements: (a) Reference measurement with 42s measurement time with a resolution of 1000x1000 pixels. (b) Fast measurement with **0.8s** measurement time with a resolution of 450x450 pixels. (ISE)*

determine an R_S-PL image. The remaining 400ms were lost during readout of the images, which is currently unavoidable with the high-IR-quantum-efficiency CCDs available on the market.

Our investigations on local series resistance imaging methods show that: (1) The significance of the obtained quantitative series resistance values needs to be improved. Therefore, weighted averaging procedures need to be found that relate the local series resistances to global series resistance values and finally to the fill factor. Our investigations in Ref. [40] will be the basis for that. (2) The readout time in high-IR-sensitivity silicon CCD technologies needs to be improved. We already identified a possible combination of available CCD design technologies in cooperation with a leading photonic device supplier. With such a device we expect a reduction of the measurement time to 500 ms or less.

7 CONLUSIONS AND OUTLOOK

We presented a comprehensive overview over infrared imaging techniques for (electrical) silicon solar cell characterization. Recent method development, especially in minority carrier diffusion length imaging, hot-spot imaging, and series resistance imaging was reviewed. The review shows that significant improvements have been achieved in the applicability of the methods for in-line application in silicon solar cell production. It was demonstrated that quantitative values for local reverse current in hot-spots can be easily obtained in *10 milliseconds*. Quantitative series resistance images were obtained in *800 milliseconds* with a good potential to reduce the measurement time to below *500 milliseconds*.

We also reported on new insights into the nature of local series resistances and on local junction breakdown in industrial multi-crystalline (mc) silicon solar cells. The fact that we found these insights mainly by applying infrared imaging methods shows that using these methods is highly beneficial also for research and development.

8 ACKNOWLEDGEMENTS

This work was partially supported by the German Federal Ministry of Education and Research under contract no. 01SF0401 (NETZ DIAGNOSTIK) and by the German Ministry for the Environment, Nature Conservation and Nuclear Safety under contracts no. 0327650D (SolarFocus) and no. 0327616 (PVQC). The authors of

the University of New South Wales acknowledge support under the Australian Research Council's Centres of Excellence Scheme. Fruitful discussions with T. Buonassisi are gratefully acknowledged.

9 REFERENCES

1. Kasemann, M., W. Kwapil, M.C. Schubert, H. Habenicht, B. Walter, M. The, S. Kontermann, S. Rein, O. Breitenstein, J. Bauer, A. Lotnyk, B. Michl, H. Nagel, A. Schütt, J. Carstensen, H. Föll, T. Trupke, Y. Augarten, H. Kampwerth, R.A. Bardos, S. Pingel, J. Berghold, W. Warta, and S.W. Glunz. *Spatially resolved silicon solar cell characterization using infrared imaging methods*. in *IEEE Photovoltaic specialists conference*. 2008. San Diego, CA, USA. p.
2. Drozdov, N.A., A.A. Patrin, and V.D. Tkachev, *Recombination radiation on dislocations in silicon.* JETP Letters, 1976. **23**(11): p. 597.
3. Kveder, V., M. Badylevich, W. Schröter, M. Seibt, E. Steinman, and A. Izotov, *Silicon light-emitting diodes based on dislocation-related luminescence.* physica status solidi (a), 2005. **202**(5): p. 901-910.
4. Akil, N., S.E. Kerns, D.V. Kerns, A. Hoffmann, and J.P. Charles, *A multimechanism model for photon generation by silicon junctions in avalanche breakdown.* Electron Devices, IEEE Transactions on, 1999. **46**(5): p. 1022-1028.
5. Isenberg, J., S. Riepe, S.W. Glunz, and W. Warta, *Imaging method for laterally resolved measurement of minority carrier densities and lifetimes: Measurement principle and first applications.* Journal of Applied Physics, 2003. **93**(7): p. 4268-4275.
6. Bail, M., J. Kentsch, R. Brendel, and M.A. Schulz. *Lifetime mapping of Si wafers by an infrared camera [for solar cell production]*. in *Photovoltaic Specialists Conference, 2000. Conference Record of the Twenty-Eighth IEEE*. 2000. p. 99-103.
7. Trupke, T., R.A. Bardos, M.C. Schubert, and W. Warta, *Photoluminescence imaging of silicon wafers.* Appl. Phys. Lett., 2006. **89**: p. 044107.
8. Würfel, P., T. Trupke, T. Puzzer, E. Schaffer, W. Warta, and S.W. Glunz, *Diffusion lengths of silicon solar cells from luminescence images.* Journal of Applied Physics, 2007. **101**(12): p. 123110.
9. Isenberg, J. and W. Warta, *Realistic evaluation of power losses in solar cells by using thermographic methods.* Journal of Applied Physics, 2004. **95**(9): p. 5200-5209.
10. Macdonald, D., J. Tan, and T. Trupke, *Imaging interstitial iron concentrations in boron-doped crystalline silicon using photoluminescence.* Journal of Applied Physics, 2008. **103**(7): p. 073710.
11. Kveder, V., M. Badylevich, E. Steinman, A. Izotov, M. Seibt, and W. Schroter, *Room-temperature silicon light-emitting diodes based on dislocation luminescence.* Applied Physics Letters, 2004. **84**(12): p. 2106-2108.
12. Schubert, M.C., S. Riepe, S. Bermejo, and W. Warta, *Determination of spatially resolved trapping parameters in silicon with injection dependent carrier density imaging.* Journal of Applied Physics, 2006. **99**(11): p. 114908.
13. Pohl, P., J. Schmidt, K. Bothe, and R. Brendel, *Mapping of trap densities and energy levels in semiconductors using a lock-in infrared camera technique.* Applied Physics Letters, 2005. **87**: p. 142104.
14. Isenberg, J., D. Biro, and W. Warta, *Fast, contactless and spatially resolved measurement of sheet resistance by an infrared method.* Progress in Photovoltaics: Research and Applications, 2004. **12**(7): p. 539-552.
15. Pohl, P. and R. Brendel, *Infrared capacity mapping of semiconductor junctions by lock-in thermography.* Applied Physics Letters, 2005. **87**(3): p. 032104.
16. Trupke, T., E. Pink, R.A. Bardos, and M.D. Abbott, *Spatially resolved series resistance of silicon solar cells obtained from luminescence imaging.* Applied Physics Letters, 2007. **90**(9): p. 093506.
17. Hinken, D., K. Ramspeck, K. Bothe, B. Fischer, and R. Brendel. *Series resistance imaging of solar cells by voltage dependent electroluminescence*. in *International PVSEC-17*. 2007. Fukuoka, Japan. p. 5O-M3-04.
18. Ramspeck, K., K. Bothe, D. Hinken, B. Fischer, J. Schmidt, and R. Brendel, *Recombination current and series resistance imaging of solar cells by combined luminescence and lock-in thermography.* Applied Physics Letters, 2007. **90**(15): p. 153502.
19. Isenberg, J., A.S.H.v.d. Heide, and W. Warta, *Investigation of Series Resistance Losses by Illuminated Lock-In Thermography.* Prog. Photovolt: Res. Appl., 2005. **13**: p. 697–703.
20. Breitenstein, O., J.P. Rakotoniaina, A.S.H.v.d. Heide, and J. Carstensen, *Series Resistance Imaging in Solar Cells by Lock-in Thermography.* Prog. Photovolt: Res. Appl., 2005. **13**: p. 645–660.
21. Breitenstein, O., J.P. Rakotoniaina, and M.H.A. Rifai, *Quantitative evaluation of shunts in solar cells by lock-in thermography.* Progress in Photovoltaics: Research and Applications, 2003. **11**(8): p. 515-526.
22. Kasemann, M., D. Grote, B. Walter, W. Kwapil, T. Trupke, Y. Augarten, R.A. Bardos, E. Pink, M.D. Abbott, and W. Warta, *Luminescence imaging for the detection of shunts on silicon solar cells.* Progress in Photovoltaics: Research and Applications, 2008. **16**(4): p. 297-305.
23. Breitenstein, O., J. Bauer, J.-M. Wagner, and A. Lotnyk, *Imaging physical parameters of pre-breakdown sites by lock-in thermography techniques.* Progress in Photovoltaics: Research and Applications, 2008: p. submitted.
24. Ramspeck, K., K. Bothe, J. Schmidt, and R. Brendel, *Correlation between spatially resolved solar cell efficiency and carrier lifetime of multicrystalline silicon.* Journal of Materials

Science: Materials in Electronics, 2008. **DOI: 10.1007/s10854-008-9671-8**.

25. Trupke, T., *Influence of photon reabsorption on quasi-steady-state photoluminescence measurements on crystalline silicon.* Journal of Applied Physics, 2006. **100**(6): p. 063531.
26. Würfel, P., S. Finkbeiner, and E. Daub, *Generalized Planck's radiation law for luminescence via indirect transitions.* Applied Physics Materials Science & Processing, 1995. **60**(1): p. 67-70.
27. Giesecke, J., M. Kasemann, M.C. Schubert, B. Michl, M. The, W. Warta, and P. Würfel. *Determination of Minority Carrier Diffusion Lengths in Silicon Solar Cells from Photoluminescence Images*. in *Proceedings of the 23rd European Photovoltaic Solar Energy Conference*. 2008. Valencia, Spain. p. accepted.
28. Muñoz, J., E. Lorenzo, F. Martínez-Moreno, L. Marroyo, and M. García, *An investigation into hot-spots in two large grid-connected PV plants.* Progress in Photovoltaics: Research and Applications, 2008. **9999**(9999): p. early view.
29. Wagner, J.-M., J. Bauer, A. Lotnyk, and O. Breitenstein. *Pre-breakdown mechanisms in multicrystalline silicon solar cells*. in *Proceedings of the 23rd European Photovoltaic Solar Energy Conference*. 2008. Valencia, Spain. p.
30. Kwapil, W., M. Kasemann, B. Walter, and W. Warta. *Spatially Resolved Measurements of Multicrystalline Silicon Solar Cells under Reverse Bias Conditions*. in *Proceedings of the 23rd European Photovoltaic Solar Energy Conference*. 2008. Valencia, Spain. p. accepted.
31. Mahadevan, S., S.M. Hardas, and G. Suryan, *Electrical breakdown in semiconductors.* Physica Status Solidi (a), 1971. **8**(2): p. 335-374.
32. Kasemann, M., *manuscript in preparation.* 2008.
33. Buonassisi, T., A.A. Istratov, M.A. Marcus, B. Lai, Z. Cai, S.M. Heald, and E.R. Weber, *Engineering metal-impurity nanodefects for low-cost solar cells.* Nat Mater, 2005. **4**(9): p. 676-679.
34. Abbott, M.D., T. Trupke, H.P. Hartmann, R. Gupta, and O. Breitenstein, *Laser isolation of shunted regions in industrial solar cells.* Progress in Photovoltaics: Research and Applications, 2007.
35. Kasemann, M., B. Walter, C. Meinhardt, J. Ebser, W. Kwapil, and W. Warta, *Emissivity-corrected power loss calibration for lock-in thermography measurements on silicon solar cells.* Journal of Applied Physics, 2008. **103**(11): p. 113503.
36. Breitenstein, O. and M. Langenkamp. *Quantitative local analysis of I-V characteristics of solar cells by thermal methods*. in *Proceedings of the 2nd World Conference on Photovoltaic Energy Conversion*. 1998. Vienna, Austria: European Commission, Ispra, Italy, 1998. p. 1382-5.
37. Pysch, D., A. Mette, and S.W. Glunz, *A review and comparison of different methods to determine the series resistance of solar cells.* Solar Energy Materials and Solar Cells, 2007. **91**(18): p. 1698-1706.
38. Hinken, D., K. Ramspeck, K. Bothe, B. Fischer, and R. Brendel, *Series resistance imaging of solar cells by voltage dependent electroluminescence.* Applied Physics Letters, 2007. **91**: p. 182104.
39. Werner, J.H., *Schottky barrier and pn-junctionI/V plots — Small signal evaluation.* Applied Physics A: Materials Science & Processing, 1988. **47**(3): p. 291-300.
40. Michl, B., H. Nagel, M. Kasemann, J. Giesecke, S. Kontermann, M. Glatthaar, S. Rein, W. Warta, A. Schütt, J. Carstensen, and H. Föll. *Application of luminescence imaging based series resistance measurement methods in an industrial environment*. in *Proceedings of the 23rd European Photovoltaic Solar Energy Conference*. 2008. Valencia, Spain. p. accepted.
41. Aberle, A.G., S.R. Wenham, and M.A. Green, *A new method for accurate measurements of the lumped seriesresistance of solar cells.* Conference Record of the Twenty Third IEEE Photovoltaic Specialists Conference, 1993, 1993: p. 133-139.
42. Carstensen, J., A. Schütt, and H. Föll. *Cello local solar cell resistance maps: Modelling of data and correlation to solar cell efficiency*. in *Proceedings of the 22nd European Photovoltaic Solar Energy Conference*. 2007. Milan: WIP Munich. p.